



Efficient structural and energetic screening of fullerene encapsulation in a large supramolecular double decker macrocycle

FABIAN BOHLE and STEFAN GRIMME*

Mulliken Center for Theoretical Chemistry, University of Bonn, Beringstraße 4, 53115 Bonn,
Germany

(Received 1 July, accepted 11 July 2019)

Abstract: Recently, Tanaka *et al.* have synthesized an organometallic supramolecular double decker macrocycle for encapsulating fullerene C₇₀. We investigate this captivating system consisting of about 500 atoms with the robust quantum mechanical tight binding method GFN2-xTB and evaluate our computational results against an experimentally measured change in association free energy (ΔG_a). Further, GFN2-xTB was used to screen higher fullerene isomers and predict the best binding guest for this specific macrocycle.

Keywords: GFN2-xTB; fullerene; binding free energy.

INTRODUCTION

Since their discovery in 1985¹, fullerenes have sparked a wave of new developments in their application², as well as the search for understanding and generation of new supramolecular complexes³. In 2018 Tanaka *et al.* synthesized a supramolecular double decker cage macrocycle which is able to complexate fullerene C₇₀.⁴ Selective purification of fullerenes in solution using macrocyclic supramolecular receptors represents a viable strategy to tackle the low solubility of the unpolar carbon allotropes.⁴ Tanakas' receptor is based on two dibenzothiophene-salen Zn^{II}-macrocycles (**1**) (see Fig. 1). The double decker macrocyclic structure (**2**) is build up from the macrocycles (**1**) containing each four Zn^{II} metal ions and both macrocycles are joined by four nitrogen-containing pillar molecules (DABCO) connecting the square-pyramidal coordinated Zn cations. Having this large host molecule with a well-defined inner cavity at hand, the experimentalists measured the association of the 1:1 host-guest complex with C₇₀ in CHCl₃/CS₂. The association constant (K_a) was evaluated by ¹H-NMR integration to be about 180 L·mol⁻¹, corresponding to an association free energy (ΔG_a) of

* Corresponding author. E-mail: grimme@thch.uni-bonn.de
<https://doi.org/10.2298/JSC190701079B>

$-3.07 \text{ kcal}^* \cdot \text{mol}^{-1}$. Further they investigated the complexation of C_{60} and found the receptor (**2**) to be able to selectively recognize C_{70} over C_{60} through higher association.

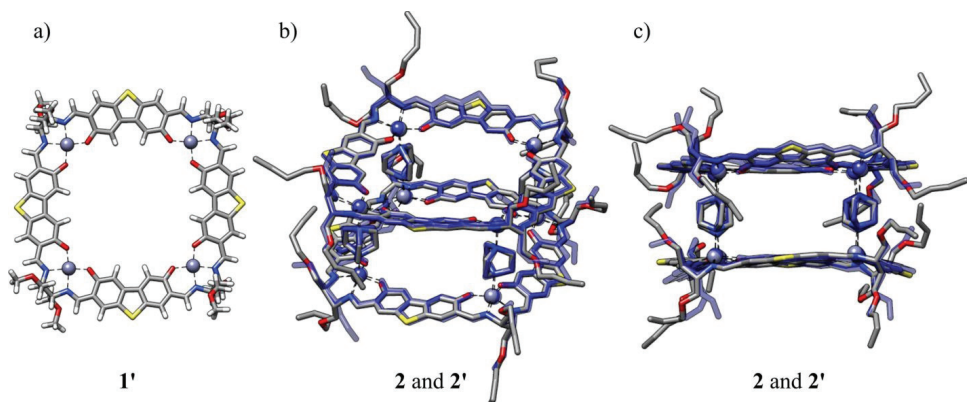


Fig. 1. a) Macrocycle **1'** geometry optimized with GFN2-xTB(GBSA); structures b) and c) show the overlay between crystal structure **2** (normal color code) and GFN2-xTB(GBSA) optimized geometry **2'** (blue color code); b) diagonal view; c) front view. In b) and c), hydrogen atoms are omitted for clarity.

The large size of supramolecular complexes clearly limits the number of applicable theoretical methods able to calculate accurate association free energies. Our current approach for systems of about a few hundred atoms is consisting of a single-structure, multi-level computational protocol, heavily relying on dispersion corrected density functional theory.^{5,6} In this paper, we are investigating the recently published quantum mechanical extended tight binding method GFN2-xTB⁷ for routinely calculating binding free energies of large supramolecular complexes in solution. GFN2-xTB compared to its predecessor GFN1-xTB⁸ is less empirical and more physically motived, *e.g.*, by including anisotropic second order density fluctuation effects. The robust method is available for all elements up to $Z = 86$ with target properties being: good geometries, vibrational frequencies and noncovalent interactions of large systems⁹. An implicit solvation model (GBSA) for describing reactions in solution is available for both GFNn-xTB methods. Although not specially parametrized for off target properties, they prove to be rather well described and the GFNn-xTB methods are currently used in the calculation of mass spectra (QCEIMS)¹⁰, in systematic conformer ensemble generations (CREST)¹¹ and in finding reaction paths for mechanistic studies (GSM/GFNn-xTB)¹².

* 1 kcal = 4184 J

COMPUTATIONAL METHODS

The initial geometries of **1** and **2** were taken from CCDC¹³ entries 1546762 and 1546764. All lower and higher fullerenes and their isomers employed in this study are following the “isolated pentagon rule” and were obtained from Tománek¹⁴. GFN2-xTB was used as implemented in the xtb code in the version 6.1. All GFN2-xTB calculations were performed with “verytight” settings and using the GBSA implicit solvation model with chloroform as the solvent. The temperature was set to 298.15 K for the thermostatistical evaluation. The intermolecular forcefield xTB-IFF¹⁵ was used from its standalone code. B97-3c¹⁶/COSMO single-point calculations were performed as implemented within the TURBOMOLE.7.2.1 program package¹⁷. More detailed information is provided in the Supplementary material to this paper.

RESULTS AND DISCUSSION

First we were interested in how well the crystal structure of **2** at the level of GFN2-xTB(GBSA(CHCl₃)) can be reproduced. For computational efficiency and to reduce the flexibility of the host molecule the R-O-*n*Bu side chains were truncated to R-OMe (**2'**), still retaining the structural properties of the original host molecule. The root mean square deviation (RMSD) between the crystal structure and **2'** GFN2-xTB(GBSA) optimized structure equals 0.77 Å. The overlay of both structures showing good correspondence is presented in Fig. 1. To investigate the complexes **2'**–C₇₀ and **2'**–C₆₀ we first need to obtain the geometry for the best intermolecular interaction. The GFN2-xTB(GBSA) optimized host and guest molecules are docked using the intermolecular forcefield xTB-IFF,¹⁵ which requires a QM potential input generated by GFNn-xTB for each monomer. The xTB-IFF-complex-geometry is subsequently reoptimized with GFN2-xTB(GBSA) to yield the final complex geometry. On all optimized geometries, free energies are calculated as the sum of the electronic energy (*E*) including the D4 dispersion correction^{18,19} in a self-consistent formulation, thermostatistical corrections (*G*_{RRHO}) calculated from vibrational frequencies and the solvation contribution (ΔG_{solv}) calculated by the implicit solvation model GBSA:

$$\Delta G_a = \Delta E + \Delta G_{\text{RRHO}}^T + \Delta G_{\text{solv}} \quad (1)$$

The association free energy is calculated from the difference of the free energies from the complex, host and guest molecules (Table I).

TABLE I. Binding free energies calculated with GFN2-xTB in comparison with experimental values. Bare interaction energies from GFN2-xTB, B97-3c(COSMO) and xTB-IFF are also given. All energies in kcal·mol⁻¹

Name	ΔE^a	ΔG_{RRHO}^a	ΔG_{solv}^a	ΔG_a^a	$\Delta G_{a,\text{exp}}^b$	ΔE B97-3c ^c	ΔE xTB-IFF
2' –C ₆₀	-38.4	18.2	13.7	-6.4	—	-27.5	-42.4
2' –C ₇₀	-43.9	19.3	17.3	-7.4	-3.07	-33.0	-50.7
1' –C ₆₀	-31.1	18.0	9.8	-3.3	—	-13.9	-26.4
1' –C ₇₀	-32.5	18.6	10.1	-3.8	—	-15.7	-28.2
2' –C ₇₈	-50.0	19.5	19.8	-10.7	—	-38.1	-58.9

^aCalculated with GFN2-xTB(GBSA(CHCl₃)); ^btaken from experiment; ^ccalculated with COSMO $\varepsilon = 4.8$

From Table I it is apparent that our calculated association free energy for $\mathbf{2}' \supset C_{70}$ is shifted compared to experiment by about 4 kcal·mol⁻¹, which can be partly attributed to the energy being calculated at tight binding level, and the implicit solvation model. For such a large complex and considering the small absolute value, the agreement is in fact satisfying. The next conclusion is that the qualitative ordering of calculated changes in free energies is correct in describing a higher association of C_{70} over C_{60} . Looking at the contributions to the changes in binding free energy, the attractive contribution mainly stems from London dispersion incorporated in the electronic energy (ΔE) and increases with larger guest size. The thermostatistical correction to the free energy has a rather constant repulsive contribution, and the positive solvation contribution to free energy clearly increases with the guest size as well. The GFN2-xTB interaction energies are benchmarked against B97-3c/COSMO(CHCl₃) DFT interaction energies. The good qualitative agreement between the semiempirical quantum chemical method and the computationally much more demanding density functional composite scheme is encouraging.

To gain more insight into the $\mathbf{2}' \supset C_{70}$ complex formation, a reaction path for the C_{70} inclusion process into the inner cavity of $\mathbf{2}'$ was calculated using the growing string method (GSM)²⁰ and GFN2-xTB(GBSA) shown in Fig. 2.

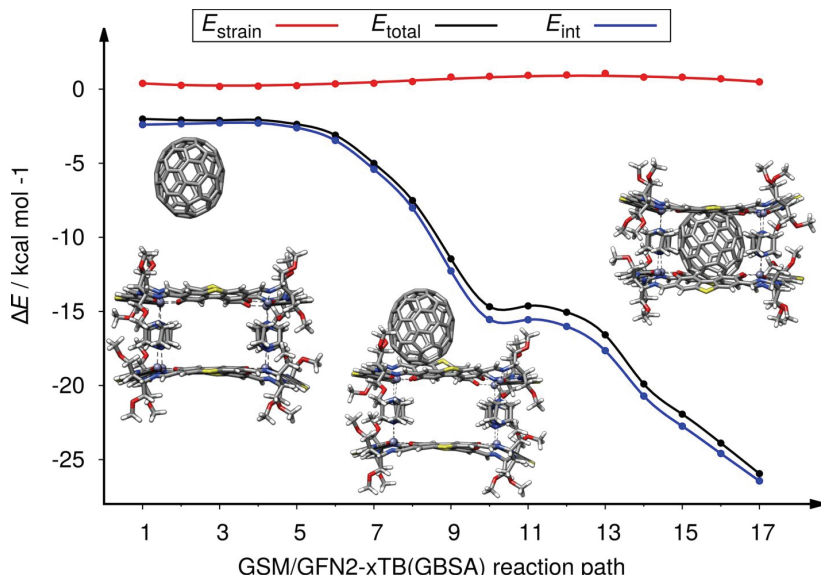


Fig. 2. GSM/GFN2-xTB(GBSA) reaction path of C_{70} entering the inner cavity of $\mathbf{2}'$.

From the reaction path no transition state could be obtained, suggesting a barrierless reaction. The calculation of the reaction path, with 20 nodes along the string, took 146 h on a single computer node with 4 cores and 3.6 GHz. Dissect-

ing the energy on the reaction path within the interaction strain model,²¹ shows almost no strain energy, *i.e.*, almost no molecular deformation and the reaction path is mainly described by the interaction energy of the fragments. Important to note is the “standing” orientation of the C₇₀ inside the cavity allowing for multiple CH-π interactions of the inward facing protons, especially at the inner rim of the macrocycles **1'**.

Knowing that C₇₀ binds to the double decker macrocycle, we searched for the best binding higher fullerene using our fast GFN2-xTB method (Fig. 3).

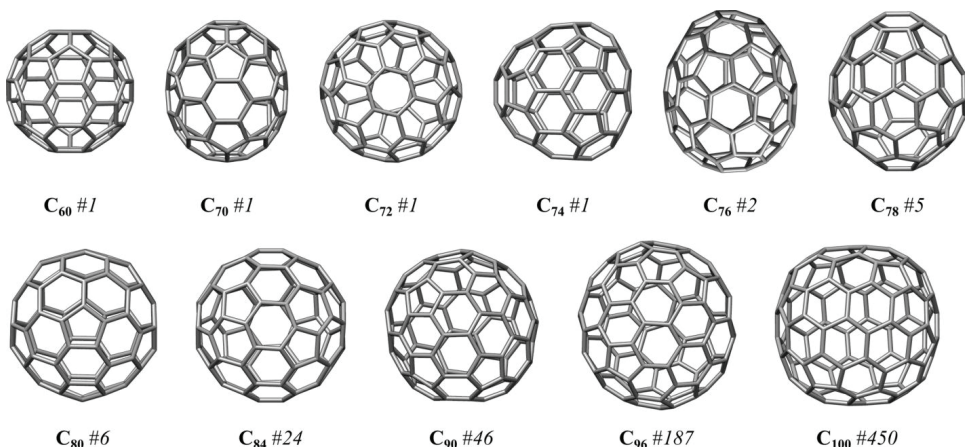


Fig. 3. Shown are lower and higher fullerene isomers having the lowest free energy determined by GFN2-xTB(GBSA), within the possible number (#) of isomers obeying the “isolated pentagon rule”.

All 724 fullerene isomers were optimized and ranked by free energy obtained from GFN2-xTB(GBSA). The lowest lying isomer was docked with the macrocycle **1'** and the double decker **2'**. The geometries were optimized, and association free energies were calculated as described above. For all complexes up to C₉₆ xTB-IFF determines the guest to be docked preferentially inside the cavity. For C₉₆ and C₁₀₀ the best guest position is determined to be outside the receptor and therefore these fullerenes were placed inside the cavity manually. Obtaining the free energy for the largest complex **2'**–C₁₀₀ took 18 h on 1 node with 14 cores (including optimization and hessian calculation). The resulting association free energies for **1'**–C_x and **2'**–C_x are shown in Fig. 4.

Analysing the associations of the fullerenes with the macrocycle **1'** it is apparent that the free energy increases with the contact surface, *e.g.*, the London dispersion, of the higher fullerenes. The best binding guest within the double decker **2'** is fullerene C₇₈ with an association free energy of –10.7 kcal·mol^{–1}.

The C₇₈ fullerene, in “standing” orientation, perfectly fills the space of the inner cavity and due to its ellipsoidal shape, similar to C₇₀, retains all CH-π

interactions of the inward facing protons. For a comparison to C_{70} the contributions to free energy are listed in Table I. Fullerenes with more carbon atoms than C_{78} are too large in size to fill the inner cavity of **2'** which is reflected in an increased Pauli repulsion and higher association free energy. The three-dimensional shape of the guest molecules in the double decker receptor has a large influence on the association which becomes apparent for C_{74} with D_{3h} symmetry.

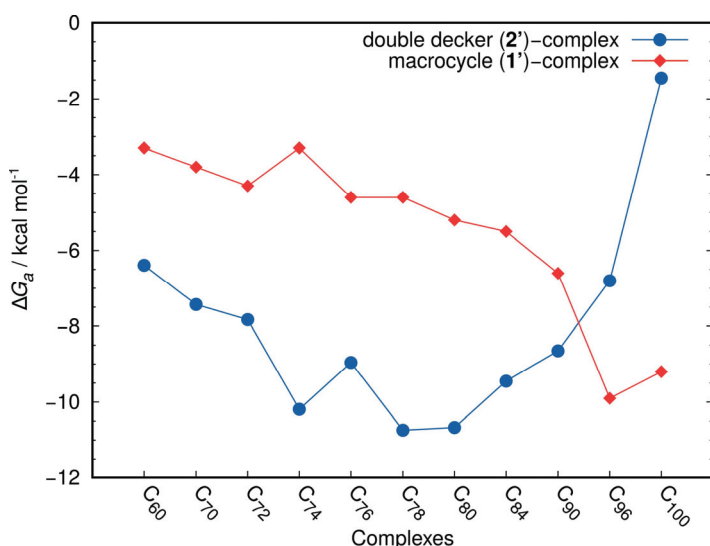


Fig. 4. Association free energies of most stable fullerene isomers with the host molecules **1'** and **2'** at GFN2-xTB(GBSA).

CONCLUSION

In this work we demonstrate that GFN2-xTB(GBSA) is capable of reproducing the experimental trend in C_{70} binding to the double decker **2'** supramolecular host by higher association compared to C_{60} . Further we have determined C_{78} to be the best interacting guest for receptor **2'**. Qualitative estimations of association free energies of large supramolecular complexes and efficient screening of various host guest systems are easily possible with GFN2-xTB. The low computational cost of the method allows it to run on a normal consumer hardware highlighting its possibilities in screening applications.

SUPPLEMENTARY MATERIAL

All geometries in *xmol* and additional computational details which are not mentioned within the manuscript are available electronically from <http://www.shd.org.rs/JSCS/>, or from the corresponding author on request.

Acknowledgements. The authors thank the DFG for funding in the framework of the priority Program No.SPP 1807 “Control of Dispersion Interactions in Chemistry”. F. B. thanks Markus Bursch for fruitful discussions. The authors declare no conflict of interest.

ИЗВОД

ЕФИКАСНИ СТРУКТУРНИ И ЕНЕРГЕТСКИ СКРИНИНГ ОБУХВАТАЊА ФУЛЕРЕНА
ВЕЛИКИМ DOUBLE DECKER ЦИКЛИЧНИМ МАКРОМОЛЕКУЛОМ

FABIAN BOHLE и STEFAN GRIMME

Mulliken Center for Theoretical Chemistry, University of Bonn, Beringstraße 4, 53115 Bonn, Germany

Tanaka са сарадницима је недавно синтетизовао органометални double decker циклични макромолекул за обухватање фулерена C₇₀. У раду истражујемо овај систем за хватање фулерена, који се састоји од око 500 атома, помоћу *tight-binding* квантно-механичке методе GFN2-xTB и процењујемо наше податке добијене на основу прорачуна према експериментално измереној слободној енергији везивања (ΔG_a). Надаље, GFN2-xTB је коришћен за анализу већих изомера фулерена и предвиђање који се фулерен најбоље везује за овај специфични циклични макромолекул.

(Примљено 1. јула, прихваћено 11. јула 2019)

REFERENCES

1. H. W. Kroto, J. R. Heath, S. C. O'Brien, R. F. Curl, R. E. Smalley, *Nature* **318** (1985) 162 (<https://doi.org/10.1038/318162a0>)
2. W. Yan, S. M. Seifermann, P. Pierrat, S. Bräse, *Org. Biomol. Chem.* **13** (2015) 25 (<https://doi.org/10.1039/C4OB01663G>)
3. F. Diederich, M. Gómez-López, *Chem. Soc. Rev.* **28** (1999) 263 (<https://doi.org/10.1039/A804248I>)
4. S. Kawano, T. Fukushima, K. Tanaka, *Angew. Chem. Int. Ed.* **57** (2018) 14827 (<https://dx.doi.org/10.1002/anie.201809167>)
5. R. Sure, S. Grimme, *J. Chem. Theory Comput.* **11** (2015) 3785 (<https://dx.doi.org/10.1021/ACS.JCTC.5B00296>)
6. R. Sure, S. Grimme, *Chem. Commun.* **52** (2016) 9893 (<https://dx.doi.org/10.1039/C6CC03664C>)
7. C. Bannwarth, S. Ehlert, S. Grimme, *J. Chem. Theory Comput.* **15** (2019) 1652 (<https://dx.doi.org/10.1021/acs.jctc.8b01176>)
8. S. Grimme, C. Bannwarth, P. Shushkov, *J. Chem. Theory Comput.* **13** (2017) 1989 (<https://dx.doi.org/10.1021/acs.jctc.7b00118>)
9. M. Bursch, H. Neugebauer, S. Grimme, *Angew. Chem. Int. Ed.* Accepted, 2019 (<https://doi.org/10.1002/anie.201904021>)
10. V. Ásgeirsson, C. A. Bauer, S. Grimme, *Chem. Sci.* **8** (2017) 4879 (<https://dx.doi.org/10.1039/C7SC00601B>)
11. S. Grimme, *J. Chem. Theory Comput.* **15** (2019) 2847 (<https://dx.doi.org/10.1021/acs.jctc.9b00143>)
12. Y.Q. Zhang, F. Bohle, R. Bleith, G. Schnakenburg, S. Grimme, A. Gansäuer, *Angew. Chem. Int. Ed.* **57** (2018) 13528 (<https://dx.doi.org/10.1002/anie.201808034>)
13. C. R. Groom, I. J. Bruno, M. P. Lightfoot, S. C. Ward, *Acta Crystallogr. B* **72** (2016) 171 (<http://dx.doi.org/10.1107/S2052520616003954>)
14. David Tománek, *Guide Through the Nanocarbon Jungle*, Morgan & Claypool Publishers, San Rafael, CA, 2014 (<http://dx.doi.org/10.1088/978-1-627-05273-3>)
15. S. Grimme, C. Bannwarth, E. Caldeweyher, J. Pisarek, A. Hansen, *J. Chem. Phys.* **147** (2017) 161708 (<https://dx.doi.org/10.1063/1.4991798>)
16. J. G. Brandenburg, C. Bannwarth, A. Hansen, S. Grimme, *J. Chem. Phys.* **148** (2018) 064104 (<https://dx.doi.org/10.1063/1.5012601>)

17. *TURBOMOLE V7.2.1 2017*, a development of University of Karlsruhe and Forschungszentrum Karlsruhe GmbH, 1989–2007, TURBOMOLE GmbH, since 2007; available from <http://www.turbomole.com>
18. E. Caldeweyher, C. Bannwarth, S. Grimme, *J. Chem. Phys.* **147** (2017) 034112 (<https://dx.doi.org/10.1063/1.4993215>)
19. E. Caldeweyher, S. Ehlert, A. Hansen, H. Neugebauer, S. Spicher, C. Bannwarth, S. Grimme, *J. Chem. Phys.* **150** (2019) 154122 (<https://dx.doi.org/10.1063/1.5090222>)
20. P. M. Zimmerman, *J. Chem. Phys.* **138** (2013) 184102 (<https://dx.doi.org/10.1063/1.4804162>)
21. W.-J. van Zeist, F. M. Bickelhaupt, *Org. Biomol. Chem.* **8** (2010) 3118 (<https://dx.doi.org/10.1039/b926828f>).



SUPPLEMENTARY MATERIAL TO
**Efficient structural and energetic screening of fullerene
encapsulation in a large supramolecular double decker
macrocycle**

FABIAN BOHLE and STEFAN GRIMME*

Mulliken Center for Theoretical Chemistry, University of Bonn, Beringstraße 4, 53115 Bonn,
Germany

J. Serb. Chem. Soc. 84 (8) (2019) 837–844

GFN2-xTB: 6

Version 6.1 of GFN2-xTB¹ was used, as implemented in the *xtb* code. All GFN2-xTB calculations were carried out with the GBSA implicit solvation model and CHCl₃ as solvent. For all calculations (optimizations and hessian calculations) the ‘very tight’ settings were used (verytight: E_{conv} (energy convergence) = $10^{-7} E_h$; G_{conv} (gradient convergence) = $2 \times 10^{-4} E_h \cdot \alpha^{-1}$; accuracy (for integral cutoffs and SCF criteria) = 0.05). Vibrational frequencies were calculated for thermostatistical correction to free energy and to verify that the optimized geometries are indeed minimum structures on the electronic potential hypersurface (check for no imaginary modes). The thermostatistical contributions to free energy are calculated in the rigid-rotor-harmonic-oscillator approach (RRHO)² and include zero point vibrational energies at 298.15 K. To reduce the error of the harmonic approximation for low-lying vibrational frequencies as well as numerical noise in the calculations, the RRHO-scheme (an interpolation between the rigid-rotor (RR)- to the harmonic oscillator (HO) is applied at low-lying frequencies (every vibrational mode below 50 cm⁻¹).

xTB-IFF

The intermolecular forcefield xTB-IFF³ is implemented in a standalone code called *xtbiff* and is generated from ‘low cost’ quantum mechanical (QM) input data (atomic partial charges, localized molecular orbitals and frontier orbital energies and densities have to be provided), here generated by GFN2-xTB(GBSA(CHCl₃)). The QM data from each fragment is used to dock the intermolecular fragments and generate the best docking position. The docking

* Corresponding author. E-mail: grimme@thch.uni-bonn.de

itself is run in gas phase, but the provided QM input data is generated within the GBSA implicit solvation model. xTB-IFF returns the intermolecular interaction energy and several docking geometries sorted by their interaction energies. Since only rigid fragments are docked, the best xTB-IFF geometry has to be optimized once more by GFN2-xTB(GBSA).

B97-3c/COSMO reference calculations

B97-3c/COSMO($\epsilon = 4.8$)⁴ reference single-point calculations were performed with the TURBOMOLE 7.2.1 program package.⁵ The resolution-of-identity (RI) approximation for Coulomb integrals was generally applied⁶ using the matching default auxiliary basis sets.⁷ The integration of the exchange-correlation contribution was performed on the numerical quadrature grids *m4*. The default convergence criteria for single-points [$10^{-7} E_h$] was applied. To be able to compare to the GFN2-xTB(GBSA) calculations the implicit solvent model COSMO was applied.

Reaction path calculation

The reaction path is calculated to get a good guess on the transition state structure. To start from reasonable geometries reactants and products are optimized with GFN2-xTB(GBSA(CHCl₃)). The reaction path is then calculated with the growing string method GSM⁸ using GFN2-xTB(GBSA(CHCl₃)) as the underlying electronic structure method. The reaction path was calculated with 20 nodes on the reaction string. Geometries close to the estimated transition state were picked and Hessians were calculated to find the imaginary mode of the transition state. On the examined reaction path no transition state could be obtained (no single imaginary mode was obtainable).

TABLE S-I. Lowest lying fullerene isomers determined by GFN2-xTB(GBSA(CHCl₃)) free energy

Fullerene isomer name within the manuscript	Fullerene name from Tomanek's, ⁹ ESI
C ₆₀	C ₆₀
C ₇₀	C ₇₀
C ₇₂	C _{72-D6d}
C ₇₄	C _{74-D3h}
C ₇₆	C _{76-D2}
C ₇₈	C _{78-C2v-3}
C ₈₀	C _{80-D5h-6}
C ₈₄	C _{84-D2-22}
C ₉₀	C _{90-C2-45}
C ₉₆	C _{96-D2-183}
C ₁₀₀	C _{100-D2-449}

REFERENCES

1. C. Bannwarth, S. Ehlert, S. Grimme, *J. Chem. Theory Comput.* **15** (2019) 165251 (<https://dx.doi.org/10.1021/acs.jctc.8b01176>)
2. S. Grimme, *Chem. Eur. J.* **18** (2012) 9955 (<https://dx.doi.org/10.1002/chem.201200497>)
3. S. Grimme, C. Bannwarth, E. Caldeweyher, J. Pisarek, A. Hansen, *J. Chem. Phys.* **147** (2017) 161708 (<https://dx.doi.org/10.1063/1.4991798>)
4. J. G. Brandenburg, C. Bannwarth, A. Hansen, S. Grimme, *J. Chem. Phys.* **148** (2018) 064104 (<https://dx.doi.org/10.1063/1.5012601>)
5. *TURBOMOLE V7.2.1 2017*, a development of University of Karlsruhe and Forschungszentrum Karlsruhe GmbH, 1989–2007, TURBOMOLE GmbH, since 2007; available from <http://www.turbomole.com>
6. K. Eickorn, O. Treutler, H. Öhm, M. Häser, R. Ahlrichs, *Chem. Phys. Lett.* **242** (1995) 652 ([https://dx.doi.org/10.1016/0009-2614\(95\)00838-U](https://dx.doi.org/10.1016/0009-2614(95)00838-U))
7. F. Weigend, *Phys. Chem. Chem. Phys.* **8** (2006) 1057 (<https://dx.doi.org/10.1039/b515623h>)
8. P. M. Zimmerman, *J. Chem. Phys.* **138** (2013) 184102 (<https://dx.doi.org/10.1063/1.4804162>)
9. D. Tománek, *Guide Through the Nanocarbon Jungle*, Morgan & Claypool Publishers, San Rafael, CA, 2014 (<http://dx.doi.org/10.1088/978-1-627-05273-3>).